ASTRONOMICAL SOCIETY OF THE PACIFIC
CONFERENCE SERIES

Volume 453

ADVANCES IN COMPUTATIONAL ASTROPHYSICS: METHODS, TOOLS AND OUTCOMES

Proceedings of a conference held at
Cefalù, Italy
13–17 June 2011

Edited by

R. Capuzzo-Dolcetta
Dep. of Physics, Sapienza, Università di Roma, Italy

M. Limongi
Istituto Nazionale di Astrofisica - Osservatorio Astronomico di Roma

A. Tornambè
Istituto Nazionale di Astrofisica - Osservatorio Astronomico di Roma

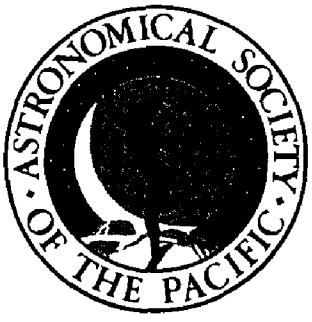

SAN FRANCISCO

ADVANCES IN COMPUTATIONAL ASTROPHYSICS: METHODS, TOOLS, AND OUTCOMES
ASP Conference Series, Vol. 453
R. Capuzzo-Dolcetta, M. Limongi & A. Tornambè, eds.

Binary Neutron Star Mergers Naturally form Jets that can Power Short Gamma-Ray Bursts

L. Rezzolla[1,2]

[1]*Max-Planck-Institut für Gravitationsphysik, Albert-Einstein-Institut, Potsdam Germany*

[2]*Department of Physics and Astronomy, Louisiana State University, Baton Rouge, LA USA*

Abstract. Short Gamma-Ray Bursts (SGRB) are among the most energetic explosions in the universe, releasing in less than a second the energy emitted by the whole Galaxy over one year. Despite decades of observations, the nature of their "central engine", where the physical conditions are the most extreme, remains largely obscure. Here we show that, starting from generic initial conditions consisting of a binary system of magnetized neutron stars in full general relativity, the final fate of the system is a rapidly spinning black hole (BH) surrounded by a hot and highly magnetized torus feeding a jet with half opening-angle of ~ 30 deg. In particular, performing simulations on timescales four times longer than previous ones, we show that magnetohydrodynamical instabilities developing after BH formation amplify an initial turbulent magnetic field of $\sim 10^{12}$ G, to produce an ordered jet along the BH spin axis with strengths $\sim 10^{15}$ G. The formation of this configuration from *abinitio* calculations provides strong evidence that the merger of neutron-star (NS) binaries is potentially behind the central engine of a SGRB. We anticipate that our study will set the basis for the realistic description of the physics behind one the most extreme phenomena in the universe.

1. Introduction

The numerical investigation of the inspiral and merger of binary NSs in full general relativity has made big strides in recent years. Crucial improvements in the formulation of the equations and numerical methods, along with increased computational resources, have extended the scope of early simulations. These developments have made it possible to increase the accuracy and to compute the full evolution up to BH formation (Baiotti et al. 2008; Yamamoto et al. 2008), without and with magnetic fields (Anderson et al. 2008; Liu et al. 2008; Giacomazzo et al. 2009; Giacomazzo et al. 2011), with idealized and realistic cold EOSs (Rezzolla et al. 2010). This tremendous progress is providing the entire gravitational waveform, from the early inspiral up to the ringing of the formed BH, supplying essential information about the signal (Baiotti et al. 2010). Advanced interferometric detectors starting from 2014 will observe these sources at an impressive rate of $\sim 40 - 400$ events per year (Abadie et al. 2010).

These simulations also serve to establish whether the end-product of the merger is the central engine of SGRBs (Narayan et al. 1992; Zhang & Meszaros 2004). We recall that the prevalent scenario invoked to explain SGRBs involves the coalescence of a binary system of compact objects, *e.g.* a BH and a NS or two NSs (Nakar 2007).

After the coalescence, the merged object is expected to collapse to a BH surrounded by an accretion torus. This scenario also requires the formation of a jet, whose existence is necessary to launch a relativistic fireball with an energy of about 10^{48} erg on a timescale of $0.1 - 1$ s (Piran 2004; Lee & Ramirez-Ruiz 2007), without assuming an unrealistically-large isotropic emission.

This 21-year-old qualitative scenario (Eichler et al. 1989), is supported by the discovery of short burst in association with old stellar populations, distinct from the young massive star associations for long bursts (Fox et al. 2005; Gehrels et al. 2005; Hjorth et al. 2005; Villasenor et al. 2005; Bloom et al. 2006), and is reproduced to a good extent by fully general-relativistic simulations (Baiotti et al. 2008; Yamamoto et al. 2008; Anderson et al. 2008; Giacomazzo et al. 2009; Rezzolla et al. 2010; Liu et al. 2008; Oechslin & Janka 2007), which show that the formation of a torus of mass $M_{\rm tor} \lesssim 0.4\, M_\odot$ around a rotating BH with spin $J/M^2 \simeq 0.7-0.8$, is inevitable (Rezzolla et al. 2010). However, the simulations have so far failed to show that a jet can be produced. We provide here evidence that a jet of ultra-strong magnetic field is generated as the end-result of the merger of a generic binary of magnetized NSs.

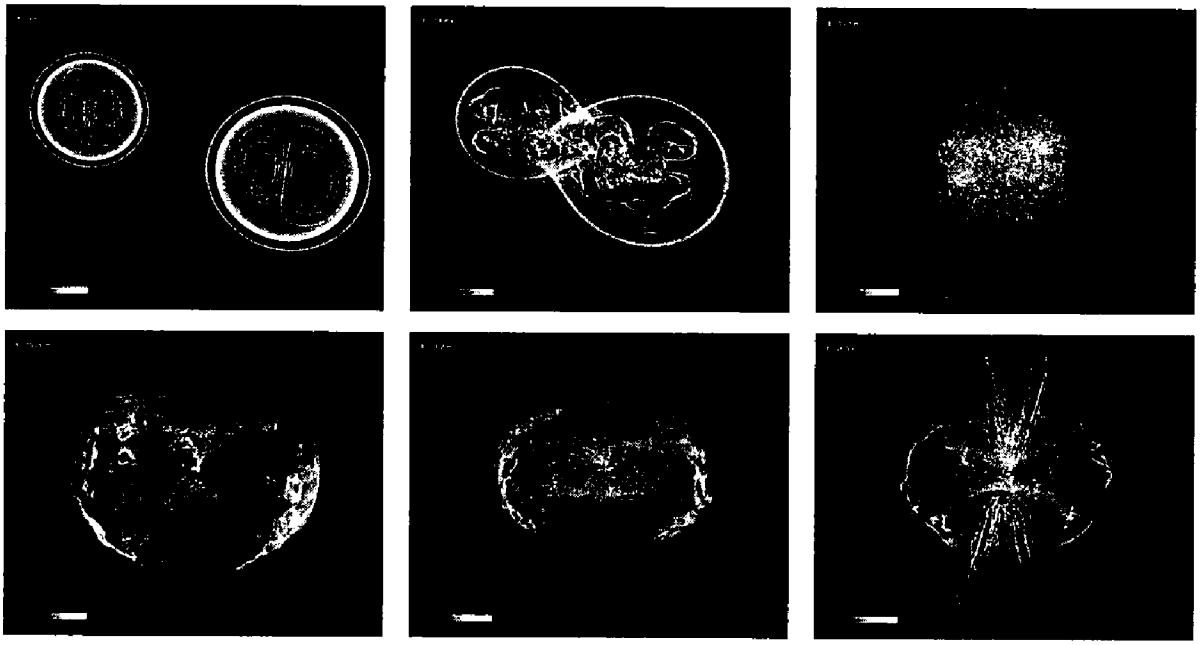

Figure 1. Snapshots at representative times of the evolution of the binary and of the formation of the jet. Shown with a color-code map is the density, over which the magnetic field lines are superposed. The panels in the upper row refer to the binary *before* the formation of the BH, namely, at the initial separation of 45 km (t = 0 ms), when the two stars merge (t = 7.4 ms), and when the HMNS evolves as a differentially rotating object (t = 13.8 ms). Shown instead in the lower row are the stages of the evolution *after* the formation of the BH, namely, soon after the collapse (t = 15.26 ms), when a toroidal magnetic fields starts being produced in the torus (t = 21.2 ms), and finally when a jet is produced (t = 26.5 ms). Figures published on *The Astrophysical Journal Letters*, 732, L6, 2011

After the coalescence, the merged object is expected to collapse to a BH surrounded by an accretion torus. This scenario also requires the formation of a jet, whose existence is necessary to launch a relativistic fireball with an energy of about 10^{48} erg on a timescale of 0.1 – 1 s (Piran 2004; Lee & Ramirez-Ruiz 2007), without assuming an unrealistically-large isotropic emission.

This 21-year-old qualitative scenario (Eichler et al. 1989), is supported by the discovery of short burst in association with old stellar populations, distinct from the young massive star associations for long bursts (Fox et al. 2005; Gehrels et al. 2005; Hjorth et al. 2005; Villasenor et al. 2005; Bloom et al. 2006), and is reproduced to a good extent by fully general-relativistic simulations (Baiotti et al. 2008; Yamamoto et al. 2008; Anderson et al. 2008; Giacomazzo et al. 2009; Rezzolla et al. 2010; Liu et al. 2008; Oechslin & Janka 2007), which show that the formation of a torus of mass $M_{\rm tor} \lesssim 0.4\, M_\odot$ around a rotating BH with spin $J/M^2 \simeq 0.7-0.8$, is inevitable (Rezzolla et al. 2010). However, the simulations have so far failed to show that a jet can be produced. We provide here evidence that a jet of ultra-strong magnetic field is generated as the end-result of the merger of a generic binary of magnetized NSs.

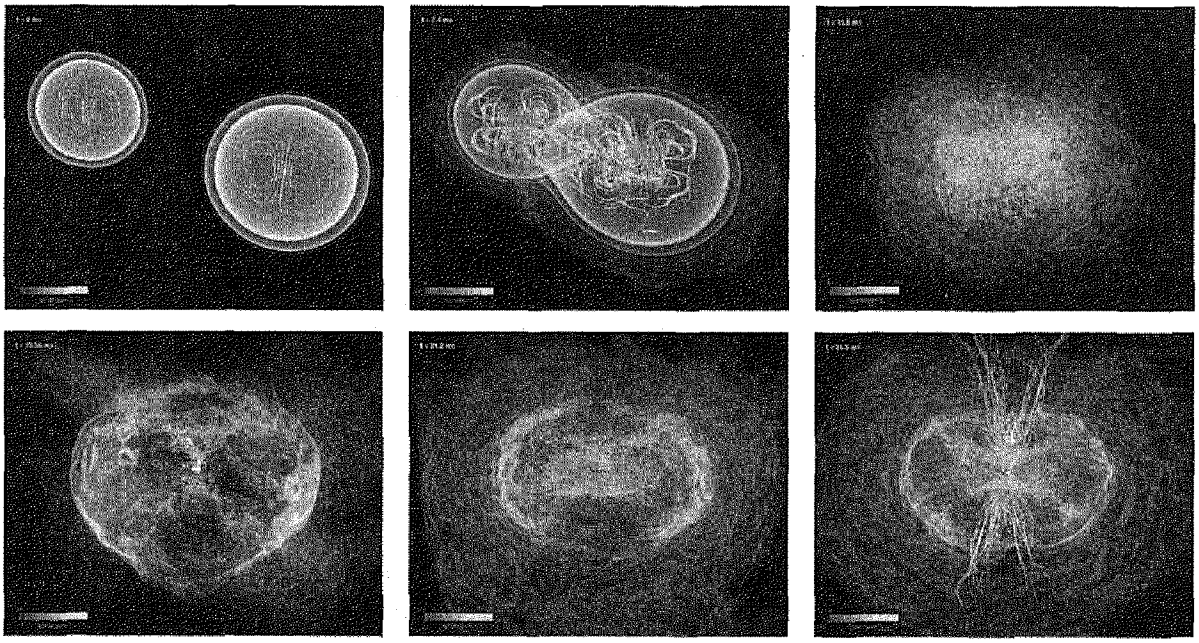

Figure 1. Snapshots at representative times of the evolution of the binary and of the formation of the jet. Shown with a color-code map is the density, over which the magnetic field lines are superposed. The panels in the upper row refer to the binary *before* the formation of the BH, namely, at the initial separation of 45 km (t = 0 ms), when the two stars merge (t = 7.4 ms), and when the HMNS evolves as a differentially rotating object (t = 13.8 ms). Shown instead in the lower row are the stages of the evolution *after* the formation of the BH, namely, soon after the collapse (t = 15.26 ms), when a toroidal magnetic fields starts being produced in the torus (t = 21.2 ms), and finally when a jet is produced (t = 26.5 ms). Figures published on *The Astrophysical Journal Letters*, 732, L6, 2011

2. Numerical Setup

Most of the details on the mathematical and numerical setup used for producing the results presented here are discussed in depth in Pollney et al. (2007); Thornburg (2004); Giacomazzo & Rezzolla (2007); Giacomazzo et al. (2009). In what follows, we limit ourselves to a brief overview. The evolution of the spacetime was obtained using the `CCATIE` code, a three-dimensional finite-differencing code providing the solution of a conformal traceless formulation of the Einstein equations (Pollney et al. 2007). The general-relativistic magnetohydrodynamics (GRMHD) equations were instead solved using the `Whisky` code (Baiotti et al. 2003, 2005; Giacomazzo & Rezzolla 2007), which adopts a flux-conservative formulation of the equations as presented by Antón et al. (2006) and high-resolution shock-capturing schemes (HRSC). As already discussed by Giacomazzo et al. (2009) the use of reconstruction schemes of high enough order is fundamental for the accurate evolution of these systems and in particular for assessing the impact of the magnetic fields. Therefore all the results presented here have been computed using the piecewise parabolic (PPM) reconstruction, while the Harten-Lax-van Leer-Einfeldt (HLLE) approximate Riemann solver (Harten et al. 1983) has been used to compute the fluxes.

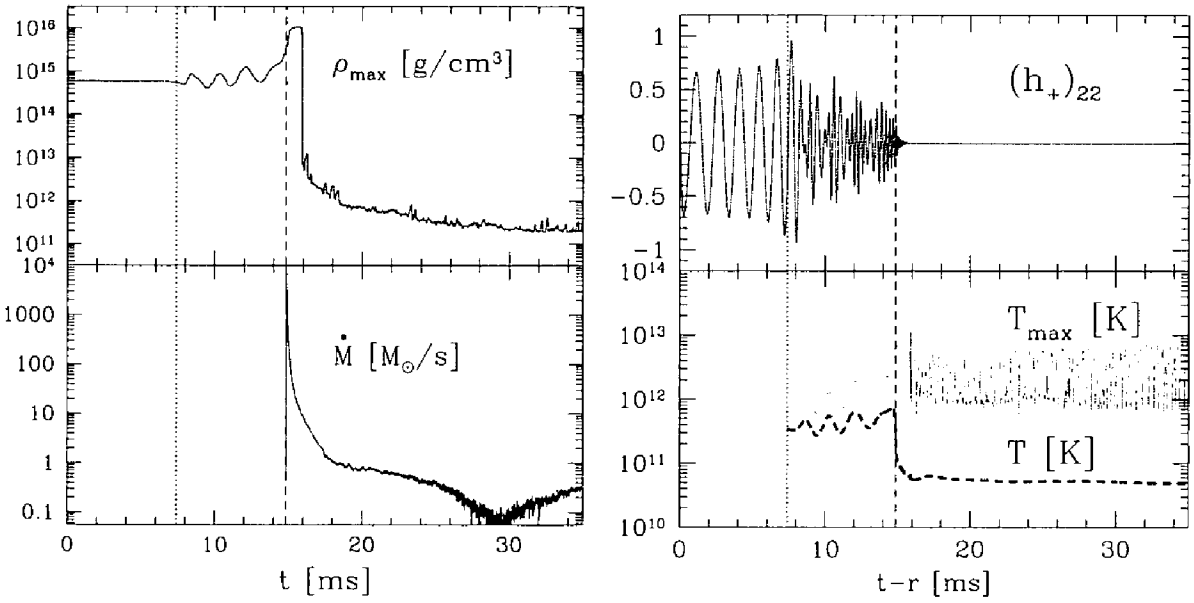

Figure 2. *Left panel:* Evolution of the maximum density (top part) and of the accretion rate onto the BH (bottom part). Shown respectively with dotted and dashed vertical lines are the times of the merger and of the formation of the BH. Note that the the maximum density remains essentially constant during the inspiral, oscillates after the merger following the contractions and expansions of the HMNS, and increases exponentially as the HMNS collapses to a BH. After this stage the values refer to the density in the torus, $\rho_{max} \simeq 10^{11}$ g/cm^3. At about the same time, the mass accretion onto the BH starts and, after an exponential decay, remains at around 10^{-1} $M_\odot$/s. *Right panel:* Evolution of the gravitational-wave signal (top part) and of the maximum (thin line) and average (thick dashed line) temperature (bottom part). Figures published on *The Astrophysical Journal Letters*, 732, L6, 2011

In order to guarantee the divergence-free character of the magnetohydrodynamic (MHD) equations we have employed the flux-CD approach described by Toth (2000),

but with the difference that we adopt as evolution variable the vector potential instead of the magnetic field. More information can be found by Giacomazzo et al. (2011), but we here simply note that since the magnetic field is computed from the curl of the vector potential using the same differential operator used to compute its divergence (*i.e.* a central-difference scheme), its divergence free character is guaranteed at essentially machine precision at all times, also when using adaptive mesh refinement (AMR). The code has been validated against a series of tests in special relativity (Giacomazzo & Rezzolla 2006) and in full general relativity [see Giacomazzo & Rezzolla (2007)]. The system of GRMHD equations is closed by an equation of state (EOS) and, as discussed in detail by Baiotti et al. (2008), the choice of the EOS plays a fundamental role in the post-merger dynamics and significantly influences the survival time against gravitational collapse of the hypermassive neutron star (HMNS) produced by the merger. However, it does not have a particular influence on the results presented here besides that of determining the precise time when the HMNS collapses to a black hole (BH). More specifically, we have employed the commonly used "ideal-fluid" EOS, in which the pressure p is expressed as $p = \rho\,\epsilon(\Gamma - 1)$, where ρ is the rest-mass density, ϵ is the specific internal energy and Γ is the adiabatic exponent. Such an EOS, while simple, provides a reasonable approximation to the properties of neutron stars (NSs).

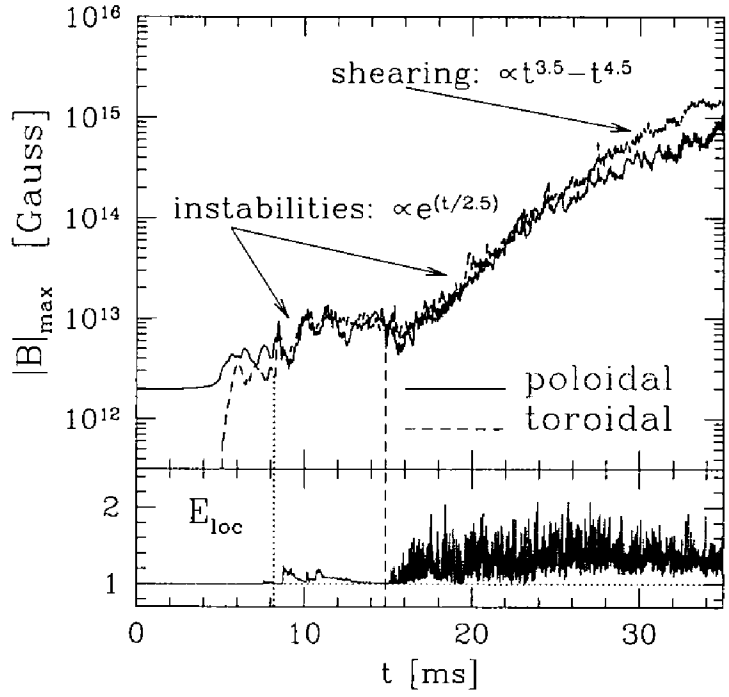

Figure 3. Evolution of the maximum of the magnetic field in its poloidal (solid line) and toroidal (dashed line) components. Note that the latter is negligibly small before the merger, but grows to about 10^{15} G by the end of the simulation. The growth of the magnetic field is either exponential, when produced by instabilities, or a power-law, when generated by shearing. The bottom panel shows instead the maximum local fluid energy indicating that an unbound outflow (*i.e.* $E_{\rm loc} > 1$) develops and is sustained after BH formation. Figures published on *The Astrophysical Journal Letters*, 732, L6, 2011

Both the Einstein and the GRMHD equations are solved using the vertex-centered AMR approach provided by the CARPET driver (Schnetter et al. 2004). Our rather ba-

sic form of AMR is based on centering the highest-resolution level around the peak in the rest-mass density of each star and moving the "boxes" following the position of this maximum as the stars orbit. The boxes are evolved as a single refinement level when they overlap. The results presented below refer to simulations performed using 6 levels of mesh refinement with the finest level having a resolution of $h = 0.1500\,M_\odot \simeq 221\,\mathrm{m}$ (where the conversion factor from mass to length is $G/c^2 \approx 7.425 \times 10^{-28}\ \mathrm{m/kg} \approx 1.477\ \mathrm{km}/M_\odot$). The grid structure is such that the size of the finest grids is $24\,M_\odot \simeq 35.4\,\mathrm{km}$, while a single refinement level covers the region between a distance $r = 164\,M_\odot \simeq 242.2\,\mathrm{km}$ and $r = 254.4\,M_\odot \simeq 375.7\,\mathrm{km}$ from the center of the domain. This region is the one in which our gravitational-wave extraction is carried out, with a resolution of $h = 4.8\,M_\odot \simeq 7.1\,\mathrm{km}$. In addition, a set of refined but fixed grids is set up at the center of the computational domain so as to better capture the details of the Kelvin-Helmholtz instability (*cf.* Baiotti et al. (2008)). Moreover, after the merger, at about 8.5ms, we enlarge the central grid that is formed by the merging of the two initial boxes. We do this in order to cover a cubical region with a side of about 88.6 km and so better resolve not only the whole HMNS, but also the BH-torus system which is produced by the collapse of the HMNS.

For all the simulations reported here we have used a reflection-symmetry condition across the $z = 0$ plane and a π-symmetry condition across the $x = 0$ plane. Stated differently, we evolve only the region $\{x \geq 0,\ z \geq 0\}$ applying a 180°-rotational-symmetry boundary condition across the plane at $x = 0$. At the outer boundary we instead used simple zeroth-order extrapolation on the MHD variables (in practice, we just copy the value of the MHD quantities from the outermost evolved point in each direction to the points of the outer boundary in that direction). Also note that a very little amount of matter and magnetic fields reaches the outer boundary, so the effect of the outer-boundary conditions on the MHD and hydrodynamical variables is negligible. The timestep on each grid is set by the Courant condition (expressed in terms of the speed of light) and so by the spatial grid resolution for that level; the Courant coefficient is set to be 0.35 on all refinement levels. The time evolution is carried out using 4th-order–accurate Runge-Kutta integration algorithm. Boundary data for finer grids are calculated with spatial prolongation operators employing 3rd-order polynomials for the matter variables and 5th-order polynomials for the spacetime variables. The prolongation in time employs 2nd-order polynomials and this ensures a significant memory saving, requiring only three time-levels to be stored, with little loss of accuracy due to the long dynamical timescale relative to the typical grid timestep.

3. Initial Data

The initial data were produced by Taniguchi and Gourgoulhon (Taniguchi & Gourgoulhon 2002) with the multi-domain spectral-method code LORENE. The initial solutions for the binaries are obtained assuming a quasi-circular orbit, an irrotational fluid-velocity field, and a conformally-flat spatial metric. The matter is modeled using a polytropic EOS $p = K\rho^\Gamma$ with $K = 123.6$ and $\Gamma = 2$, in which case the maximum gravitational mass is $M_{\rm ADM} \simeq 1.82\,M_\odot$ for a nonrotating star and $M_{\rm ADM} \simeq 2.09\,M_\odot$ for a uniformly rotating one. Since no self-consistent solution is available for magnetized binaries yet, a poloidal magnetic field is added a-posteriori using the vector potential

$$A_\phi \equiv \varpi^2 A_b \max\left(p - p_{\rm cut}, 0\right)^{n_s}, \tag{1}$$

where $\varpi \equiv \sqrt{x^2+y^2}$, $A_b > 0$ parameterizes the strength of the magnetic field, $p_{\rm cut}$ defines where in the NS the magnetic field goes to zero, and $n_{\rm s}$ determines the degree of differentiability of the potential. The components of the magnetic field are then computed by taking the curl of the Cartesian components of Eq. (1) to enforce that the divergence of the magnetic field is zero at machine precision. Here we have set $P_{\rm cut} = 0.04\,\max(P)$, and $n_{\rm s} = 2$ to enforce that both the magnetic field and its first derivative are zero at $P = P_{\rm cut}$. Anderson et al. (2008) the magnetic field was built with an expression equivalent to (1), but with $P_{\rm cut}$ set to the pressure in the atmosphere, and by Liu et al. (2008) the expression used is slightly different and $P_{\rm cut}$ is set to be $4\% - 0.1\%$ of $\max(P)$; both Anderson et al. (2008) and Liu et al. (2008) use $n_{\rm s} = 1$.

We consider a configuration that could realistically represent the properties of a binary a few orbits before coalescence. More specifically, we simulate two equal-mass NSs, each with a gravitational mass of $1.5\,M_\odot$ (sufficiently large to produce a BH soon after the merger), an equatorial radius of 13.6 km, and on a circular orbit with initial separation of 45 km. Confined in each star is a poloidal magnetic field with a maximum strength of 10^{12} G (Giacomazzo et al. 2011).

4. Results

At this separation, the binary loses large amounts of energy and angular momentum via the emission of gravitational waves, thus rapidly proceeding on tighter orbits as the evolution proceeds. After about 8 ms, or equivalently 3 orbits, the two NSs merge forming a hypermassive NS (HMNS), namely, a rapidly and differentially-rotating NS, whose mass, $3.0\,M_\odot$, is above the maximum mass, $2.1\,M_\odot$, allowed by uniform rotation. Being metastable, a HMNS can exist as long as it is able to resist against collapse via a suitable re-distribution of angular momentum [deforming into a "bar" shape (Shibata & Taniguchi 2006; Baiotti et al. 2008)], or through the increased pressure-support coming from the large temperature-increase produced by the merger. However, because the HMNS is also losing angular momentum through gravitational waves, its lifetime can only be limited to a few ms, after which it collapses to a rotating BH with mass $M = 2.91\,M_\odot$ and spin $J/M^2 = 0.81$, surrounded by a hot and dense torus with mass $M_{\rm tor} = 0.063\,M_\odot$ (Giacomazzo et al. 2011).

This is summarized in Fig. 1, which offers snapshots at representative times of the density (shown with a color-code) and of the magnetic field lines. The first four panels, in particular, refer respectively to the binary from the initial instant ($t = 0$ ms), to when the two stars merge ($t = 7.4$ ms), to when the HMNS evolves as a differential rotating bar ($t = 13.8$ ms), or to soon after the collapse to a rotating BH ($t = 15.26$ ms). The binary dynamics can also be appreciated from Fig. 2; the top part of the left panel, in particular, shows the evolution of the maximum density, while the bottom part exhibits the accretion rate once the BH is formed. The torus soon reaches a quasi-stationary regime, during which the density attains maximum values of $\sim 10^{12}\,{\rm g/cm^3}$, while the accretion rate settles to $\sim 10^{-1}\,M_\odot/{\rm s}$. Using the measured values of the torus mass and of the accretion rate, and assuming the latter will not change significantly, such a regime could last $\simeq 0.3$ s, after which the torus is fully accreted. This is long enough for the neutrinos produced in the torus to escape and annihilate in the neighborhood of the torus, depositing $\simeq 0.2 - 0.3\%$ of their energy in the gas present near the BH and thus providing the energy necessary to launch a relativistic fireball (Ruffert et al. 1997; Ruffert & Janka 1998). Because we do not account for radiative losses, this large

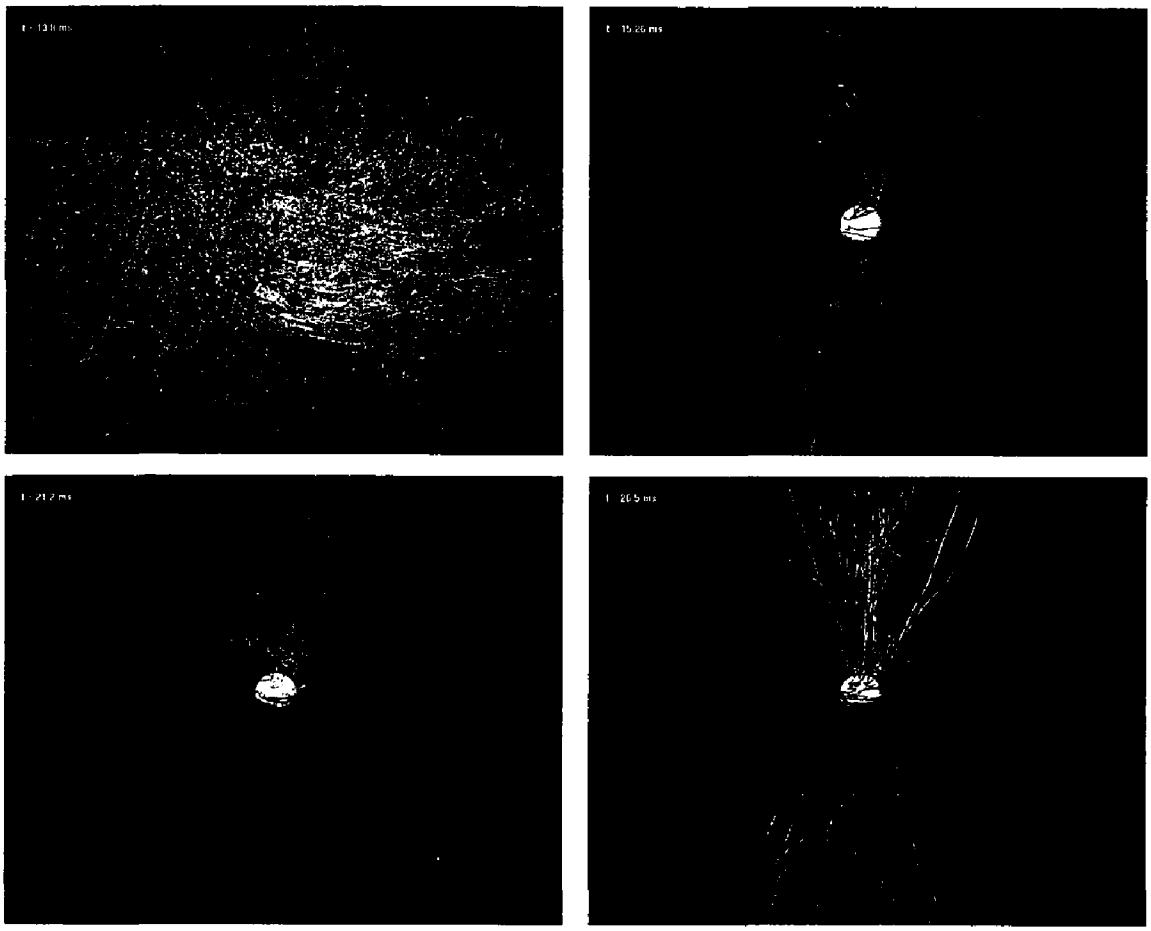

Figure 4. The same as in the last four panels of Fig. 1, but without the density contours and with a larger magnification so as to highlight the magnetic-field structure inside the torus and on the equatorial plane (green) and outside the torus and near the axis (white). The highly turbulent, predominantly poloidal magnetic-field structure in the HMNS (t = 13.8 ms) changes systematically as the BH is produced (t = 15.26 ms), leading to the formation of a predominantly toroidal magnetic field in the torus (t = 21.2 ms). Dynamo actions and instabilities then lead to the amplification of several orders of magnitude of the magnetic field and to the generation of a jet (t = 26.5 ms). Figures published on *The Astrophysical Journal Letters*, 732, L6, 2011.

reservoir of thermal energy in the torus cannot be extracted in our simulations. The top part of the right panel of Fig. 2 shows the gravitational waveform, while the bottom one exhibits the evolution of the maximum (thin line) and of the average (thick dashed line) temperature as deduced from the evolution of the internal energy and hence valid only after the merger (Baiotti et al. 2008). Both temperatures increase considerably after the merger, keeping the HMNS from collapsing immediately to a BH, but while the average one drops to $T \simeq 10^{11}$ K after BH formation, the maximum temperature (*i.e.* of the outer layers of the torus) can be as large as $T_{\rm max} \simeq 5 \times 10^{12}$ K.

The last two panels of Fig. 1 offer views of the accreting torus. Although the *matter* dynamics is quasi-stationary, the two last panels clearly show that the *magnetic-field* dynamics is far from being quasi-stationary. Indeed, this regime, which was not accessible to previous simulations (Liu et al. 2008; Giacomazzo et al. 2011), is essential for the generation of a jet. Because the strongly magnetized matter in the torus is highly

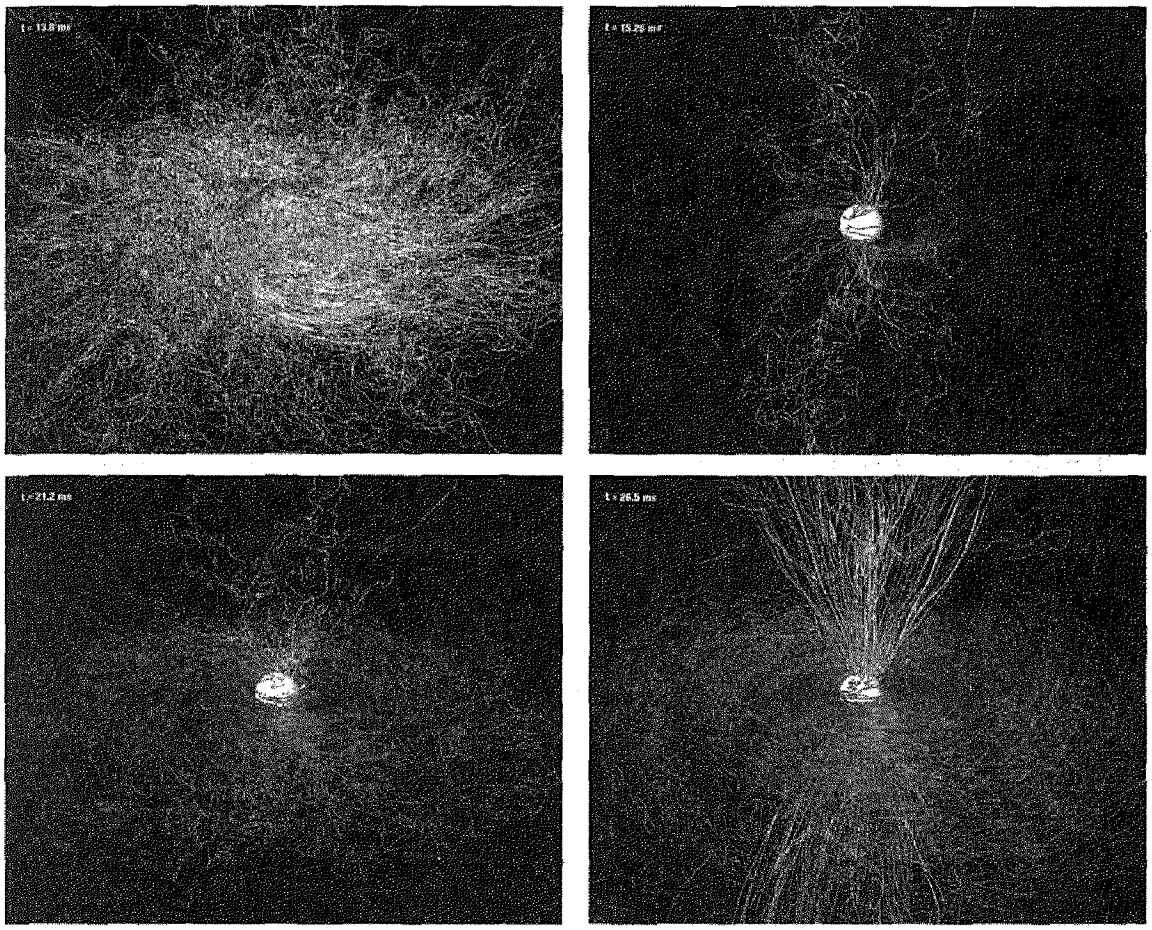

Figure 4. The same as in the last four panels of Fig. 1, but without the density contours and with a larger magnification so as to highlight the magnetic-field structure inside the torus and on the equatorial plane (green) and outside the torus and near the axis (white). The highly turbulent, predominantly poloidal magnetic-field structure in the HMNS ($t = 13.8$ ms) changes systematically as the BH is produced ($t = 15.26$ ms), leading to the formation of a predominantly toroidal magnetic field in the torus ($t = 21.2$ ms). Dynamo actions and instabilities then lead to the amplification of several orders of magnitude of the magnetic field and to the generation of a jet ($t = 26.5$ ms). Figures published on *The Astrophysical Journal Letters*, 732, L6, 2011.

reservoir of thermal energy in the torus cannot be extracted in our simulations. The top part of the right panel of Fig. 2 shows the gravitational waveform, while the bottom one exhibits the evolution of the maximum (thin line) and of the average (thick dashed line) temperature as deduced from the evolution of the internal energy and hence valid only after the merger (Baiotti et al. 2008). Both temperatures increase considerably after the merger, keeping the HMNS from collapsing immediately to a BH, but while the average one drops to $T \simeq 10^{11}$ K after BH formation, the maximum temperature (*i.e.* of the outer layers of the torus) can be as large as $T_{\rm max} \simeq 5 \times 10^{12}$ K.

The last two panels of Fig. 1 offer views of the accreting torus. Although the *matter* dynamics is quasi-stationary, the two last panels clearly show that the *magnetic-field* dynamics is far from being quasi-stationary. Indeed, this regime, which was not accessible to previous simulations (Liu et al. 2008; Giacomazzo et al. 2011), is essential for the generation of a jet. Because the strongly magnetized matter in the torus is highly

conductive, it shears the magnetic-field lines via differential rotation. A measurement of the angular-velocity in the torus indicates that it is Keplerian to a very good precision and thus unstable to the magneto-rotational instability (MRI) (Balbus & Hawley 1998), which develops $\simeq 5$ ms after BH formation and amplifies exponentially both the poloidal and the toroidal magnetic fields; the e-folding time of the instability is $\simeq 2.5$ ms and in good agreement with the one expected in the outer parts of the torus (Balbus & Hawley 1998). Because of this exponential growth, the final value of the magnetic field is largely insensitive to the initial strength and thus a robust feature of the dynamics.

A quantitative view of the magnetic-field growth is shown in Fig. 3, which shows the evolution of the maximum values of the magnetic field in its poloidal and toroidal components. Note that the latter is negligibly small before the merger, reaches equipartition with the poloidal field as a result of a Kelvin-Helmholtz instability triggered by the shearing of the outer layers at the merger (Giacomazzo et al. 2011), and finally grows to about 10^{15} G by the end of the simulation. At later times, *i.e.* for $t \gtrsim 22$ ms, when the instability is suppressed, the further growth of the field is due to the shearing of the field lines and it increases only as a power-law with exponent 3.5/4.5 for the poloidal/toroidal component, eventually stalling after $t \simeq 35$ ms. Also shown in the bottom panel of Fig. 3 is the maximum local fluid energy, highlighting that an *unbound outflow* (*i.e.* $E_{\rm loc} > 1$) develops after BH formation and persists for the whole duration of the simulation. Figure 3 also explains why these results represent a breakthrough: only when the dynamics of the BH and of the magnetized torus are continued on timescales that are about 4 times longer than previous ones (Liu et al. 2008), can instabilities develop and generate the jet.

Finally, Fig. 4 provides a synthetic and yet powerful summary of the magnetic-field dynamics. The panels refer to the same times as in Fig. 1, but do not show the density and have a larger magnification to highlight the magnetic-field structure inside the torus and on the equatorial plane (green), and outside the torus and near the axis (white). It is apparent that the highly turbulent magnetic field in the HMNS ($t = 13.8$ ms) changes systematically as the BH is produced ($t = 15.26$ ms), leading to the formation of a toroidal magnetic field in the torus ($t = 21.2$ ms). As the MRI sets in, the magnetic field is not only amplified, but also organizes itself into a dual structure, which is mostly toroidal in the torus with $B_{\rm tor} \sim 2 \times 10^{15}$ G, but predominantly poloidal and jet-like along the spin axis of the BH, with $B_{\rm pol} \sim 8 \times 10^{14}$ G ($t = 26.5$ ms).

The jet has a semi opening-angle of ~ 30 deg and is magnetically dominated as indicated by the ratio of the gas-to-magnetic-pressures $\beta \equiv p_{\rm gas}/p_{\rm mag}$, which evolves from having average values $\beta \simeq 10^6 - 10^7$ before the merger, to having minimum values $\beta \simeq 10^{-1} - 10^{-2}$ after the formation of the BH. The neighborhood of the jet is also where the flow is mostly outward-pointing, with Lorentz factors that are not very high ($\Gamma \lesssim 4$), but can be easily amplified by several orders of magnitude through special-relativistic effects (Aloy & Rezzolla 2006; Mizuno et al. 2009; Komissarov et al. 2010) or the variability of the flow (Granot et al. 2010).

The calculations reported here are both the most complete and the computationally most expensive performed to date to model the central engine of SGRBs. By showing the generation of a jet and of relativistic outflows, they reveal that a non-isotropic emission is inevitable in SGRBs and thus lift an important veil still covering the properties of the central engine. Yet, they lack a proper treatment of the energy losses via photons and neutrinos, which can provide a fundamental contribution to the energy-input necessary to launch the fireball and cool the torus (Ruffert et al. 1997; Ruffert & Janka

1998), . When future work will be able to include these contributions in a consistent general-relativistic context, another veil will be lifted, possibly exposing the central engine.

Acknowledgments. The work reported here has been made in collaboration with Bruno Giacomazzo, Luca Baiotti, Jonathan Granot, Chryssa Kouveliotou, Miguel A. Aloy. A good part of it has been published on *The Astrophysical Journal Letters, 732, L6, 2011 May 1.*
It is a pleasure to thank M. Koppitz for the visualization of the results. The computations were performed on the Damiana Cluster at the AEI. This work was supported in part by the DFG grant SFB/Transregio 7, by "CompStar", a Research Networking Programme of the European Science Foundation, by the MEXT Grant-in-Aid for Young Scientists (22740163) and by NASA grant number NNX09AI75G.
Additional material in terms of animations can be found on the webpages of the numerical-relativity group at the Albert Einstein Institute
`http://numrel.aei.mpg.de/images/relativistic-binary-neutron-star-inspirals`
and on the public-outreach webpages of NASA
`http://www.nasa.gov/topics/universe/features/gamma-ray-engines.html`.

References

Abadie, J., Abbott, B. P., Abbott, R., Abernathy, M., Accadia, T., Acernese, F., Adams, C., Adhikari, R., Ajith, P., Allen, B., & et al. 2010, Classical and Quantum Gravity, 27, 173001. 1003.2480
Aloy, M. A., & Rezzolla, L. 2006, Astrophys. J., 640, L115
Anderson, M., Hirschmann, E. W., Lehner, L., Liebling, S. L., Motl, P. M., Neilsen, D., Palenzuela, C., & Tohline, J. E. 2008, Phys. Rev. Lett., 100, 191101. 0801.4387
Antón, L., Zanotti, O., Miralles, J. A., Martí, J. M., Ibáñez, J. M., Font, J. A., & Pons, J. A. 2006, Astrophys. J., 637, 296. astro-ph/0506063
Baiotti, L., Damour, T., Giacomazzo, B., Nagar, A., & Rezzolla, L. 2010, Phys. Rev. Lett., 105, 261101. 1009.0521
Baiotti, L., Giacomazzo, B., & Rezzolla, L. 2008, Phys. Rev. D, 78, 084033. 0804.0594
Baiotti, L., Hawke, I., Montero, P., & Rezzolla, L. 2003, in Computational Astrophysics in Italy: Methods and Tools, edited by R. Capuzzo-Dolcetta (Trieste: MSAIt), vol. 1, 210
Baiotti, L., Hawke, I., Montero, P. J., Löffler, F., Rezzolla, L., Stergioulas, N., Font, J. A., & Seidel, E. 2005, Phys. Rev. D, 71, 024035
Balbus, S. A., & Hawley, J. F. 1998, Reviews of Modern Physics, 70, 1
Bauswein, A., Janka, H., & Oechslin, R. 2010, Phys. Rev. D, 82, 084043. 1006.3315
Bloom, J. S., & et al. 2006, Astrophysical Journal, 638, 354. arXiv:astro-ph/0505480
Dessart, L., Ott, C. D., Burrows, A., Rosswog, S., & Livne, E. 2009, Astrophys. J., 690, 1681. 0806.4380
Eichler, D., Livio, M., Piran, T., & Schramm, D. N. 1989, Nature, 340, 126
Fox, D. B., & et al. 2005, Nature, 437, 845
Gehrels, N., & et al. 2005, Nature, 437, 851.
Giacomazzo, B., & Rezzolla, L. 2006, Journal of Fluid Mechanics, 562, 223.
— 2007, Class. Quantum Grav., 24, S235.
Giacomazzo, B., Rezzolla, L., & Baiotti, L. 2009, Mon. Not. R. Astron. Soc., 399, L164
Giacomazzo, B., Rezzolla, L., & Baiotti, L. 2011, Phys. Rev. D, 83, 044014
Granot, J., Komissarov, S., & Spitkovsky, A. 2010, arXiv:1004.0959
Harten, A., Lax, P. D., & van Leer, B. 1983, SIAM Rev., 25, 35

Hjorth, J., Watson, D., Fynbo, J. P. U., Price, P. A., Jensen, B. L., Jørgensen, U. G., Kubas, D., Gorosabel, J., Jakobsson, P., Sollerman, J., Pedersen, K., & Kouveliotou, C. 2005, Nature, 437, 859.
Joshua A. Faber, F. A. R., Philippe Grandclément 2004, Phys. Rev. D, 69, 124036
Komissarov, S. S., Vlahakis, N., & Königl, A. 2010, Mon. Not. R. Astron. Soc., 407, 17.
Lee, W. H., & Ramirez-Ruiz, E. 2007, New J. Phys., 9, 17.
Liu, Y. T., Shapiro, S. L., Etienne, Z. B., & Taniguchi, K. 2008, Phys. Rev. D, 78, 024012
Liu, Y. T., Shapiro, S. L., Etienne, Z. B., & Taniguchi, K. 2008, Phys. Rev. D, 78, 024012.
Mizuno, Y., et al. 2009, Astrophys. J. Lett., 690, L47
Nakar, E. 2007, Phys. Rep., 442, 166.
Narayan, R., Paczynski, B., & Piran, T. 1992, Astrophys. J., 395, L83
Oechslin, R., & Janka, H. T. 2006, Mon. Not. R. Astron. Soc., 368, 1489
— 2007, Phys. Rev. Lett., 99, 121102
Oechslin, R., Janka, H. T., & Marek, A. 2007, Astron. Astrophys., 467, 395
Oechslin, R., Rosswog, S., & Thielemann, F. K. 2002, Phys. Rev. D, 65, 103005
Piran, T. 2004, Rev. Mod. Phys., 76, 1143
Pollney, D., Reisswig, C., Rezzolla, L., Szilágyi, B., Ansorg, M., Deris, B., Diener, P., Dorband, E. N., Koppitz, M., Nagar, A., & Schnetter, E. 2007, Phys. Rev. D, 76, 124002
Rezzolla, L., Baiotti, L., Giacomazzo, B., Link, D., & Font, J. A. 2010, Class. Quantum Grav., 27, 114105.
Rosswog, S., & Liebendörfer, M. 2003, Mon. Not. R. Astron. Soc., 342, 673.
Rosswog, S., Ramirez-Ruiz, E., & Davies, M. B. 2003, Mon. Not. R. Astron. Soc., 345, 1077.
Ruffert, M., & Janka, H.-T. 1998, Astron. Astrophys., 338, 535
Ruffert, M., Janka, H.-T., & Schäfer, G. 1996, Astron. Astrophys., 311, 532
Ruffert, M., Janka, H.-T., Takahashi, K., & Schaefer, G. 1997, Astron. Astrophys., 319, 122
Schnetter, E., Hawley, S. H., & Hawke, I. 2004, Class. Quantum Grav., 21, 1465
Shibata, M., & Taniguchi, K. 2006, Phys. Rev. D, 73, 064027
Shibata, M., Taniguchi, K., & Uryū, K. 2005, Phys. Rev. D, 71, 084021.
Taniguchi, K., & Gourgoulhon, E. 2002, Phys. Rev. D, 66, 104019
Thornburg, J. 2004, Class. Quantum Grav., 21, 743.
Toth, G. 2000, J. Comput. Phys., 161, 605
Villasenor, J. S., & et al. 2005, Nature, 437, 855.
Yamamoto, T., Shibata, M., & Taniguchi, K. 2008, Phys. Rev. D, 78, 064054.
Zhang, B., & Meszaros, P. 2004, Int. J. Mod. Phys. A, 19, 2385